




# Statistical Analysis of Precipitation Extremes in São Francisco River Basin, Brazil

Nayara Arroxelas dos Santos Siqueira<sup>1</sup> , Anderlan Henrique Batista Siqueira<sup>2</sup> ,  
Augusto José Pereira Filho<sup>1</sup> 

<sup>1</sup>Departamento de Ciências Atmosféricas, Instituto de Astronomia, Geofísica e Ciências Atmosféricas, Universidade de São Paulo, São Paulo, Brazil

<sup>2</sup>Instituto de Ciências Atmosféricas, Universidade Federal de Alagoas, Alagoas, Brazil

Email: nayara.arroxelas@gmail.com, augusto.pereira@iag.usp.br, anderlansiqueira@gmail.com

**How to cite this paper:** dos Santos Siqueira, N.A., Siqueira, A.H.B. and Pereira Filho, A.J. (2022) Statistical Analysis of Precipitation Extremes in São Francisco River Basin, Brazil. *Atmospheric and Climate Sciences*, 12, 383-408.

<https://doi.org/10.4236/acs.2022.122023>

**Received:** February 15, 2022

**Accepted:** April 9, 2022

**Published:** April 12, 2022

Copyright © 2022 by author(s) and Scientific Research Publishing Inc. This work is licensed under the Creative Commons Attribution International License (CC BY 4.0).

<http://creativecommons.org/licenses/by/4.0/>



Open Access

## Abstract

This study comprises a climatology of the spatial variability of precipitation over the São Francisco River Basin (SFRB), characterized by its geographic heterogeneity. The different rainfall regimes in the region were analyzed through statistical and spectral analyses. Measured precipitation data, Pacific Decennial Climate indexes, ENSO, Atlantic Multidecadal Oscillation, North Atlantic Oscillation, Atlantic dipole, and the sunspot cycle over 65 years were used. The rainfall data were filtered and filled in using the regional weighting method. The spatial and temporal variability of precipitation along the SFRB is remarkable. A pattern was observed along with the time series of precipitation over the SFRB. The cluster analysis identified four homogeneous regions in the SFRB and explained 87.4% of the total variance of the average monthly rainfall of the 199 rain gauges. The Cross-wavelet analysis identified the relationship between the precipitation data series and the climatic indexes that are analyzed in this work.

## Keywords

Cross-Wavelet, Statistical Analysis, Hydrometeorology, Climatology

## 1. Introduction

The hydrological cycle describes the natural flow of water in its liquid, solid and gaseous states in the atmosphere, hydrosphere, cryosphere, lithosphere, and biosphere. Water volumes vary in quantity and quality through the earth's system, unlimited in the Oceans and null over large desert areas of the lithosphere [1] [2] [3].

The terrestrial branch of the hydrological cycle is of great interest at the watershed scale [4]. The watershed is a region where the precipitation converges to

an outlet through the main watercourse and its tributaries [2] [5].

The water budget in a given watershed is an important and integral part of the hydrologic cycle. Hydrology is an applied science that studies processes of adding and removing water from the solid earth [3]. Furthermore, variables such as precipitation, evapotranspiration, infiltration, percolation, runoff, and streamflow are complex phenomena of watershed hydrology subject to qualitative and quantitative analysis [6].

The Brazilian water resources are especially important to agriculture and hydroelectric power generation, corresponding to 97% of the total electric power produced, the third-largest producer in the world [4]. Precipitation extreme events in watersheds can impact these commodities.

The five main physical components of planet earth are nonlinear systems that undergo changes such as in their thermodynamic states throughout variable time scales with fluctuations between high (low) energy states. For instance, glaciers advance and retreat as the earth's temperature increases and decrease by solar and internal variability changing Earth's climate, and also by other factors such as cosmic rays' activity that affect low clouds [7]. These factors might be related to droughts and floods. Moreover, extreme weather and climate events are related to weather and climate variability from days to millennia, events of significant impact [8].

The Brazilian legislature passed a Water Bill in 1997 to discipline water uses to guarantee its quality and quantity to the future generation and to give priority to human and animal consumption under extreme drought events [9]. Extreme droughts caused by the high divergence of water affect all anthropic activities with resulting severe social and economic impacts as fatalities and damage to the infrastructure [10]. Additional constraint impacts are related to poor government planning and inappropriate land use and occupancy [11]. Extreme weather and climate events impact the public and private sectors [12].

Brazil is one the largest countries in the world with a wild diversity of landscapes, fauna, and flora sprang from its complex climate and water availability associated with eight precipitation regimes [13]. Therefore, the SFRB is studied in this research work as a representative of Brazil's climate variability from the Southeast (colder and wetter) and Northeast (warmer and drier).

The objective of this article is to study, analyze and simulate the behavior of the precipitation field over the SFRB, and its relationship with climatic variability that interfere in the production of rain, specifically, to analyze the long- and short-term interactions with the rainfall regime of the Hydrographic Basins. Apply statistical techniques to qualify and, if possible, quantify the dynamics of precipitation in the region studied. Study extreme events using statistical methods and correlate with atmospheric and oceanic oscillations.

## 2. Material and Methods

### 2.1. Study Area

The SFRB shown in **Figure 1** has an area of 638,000 km<sup>2</sup> located between the

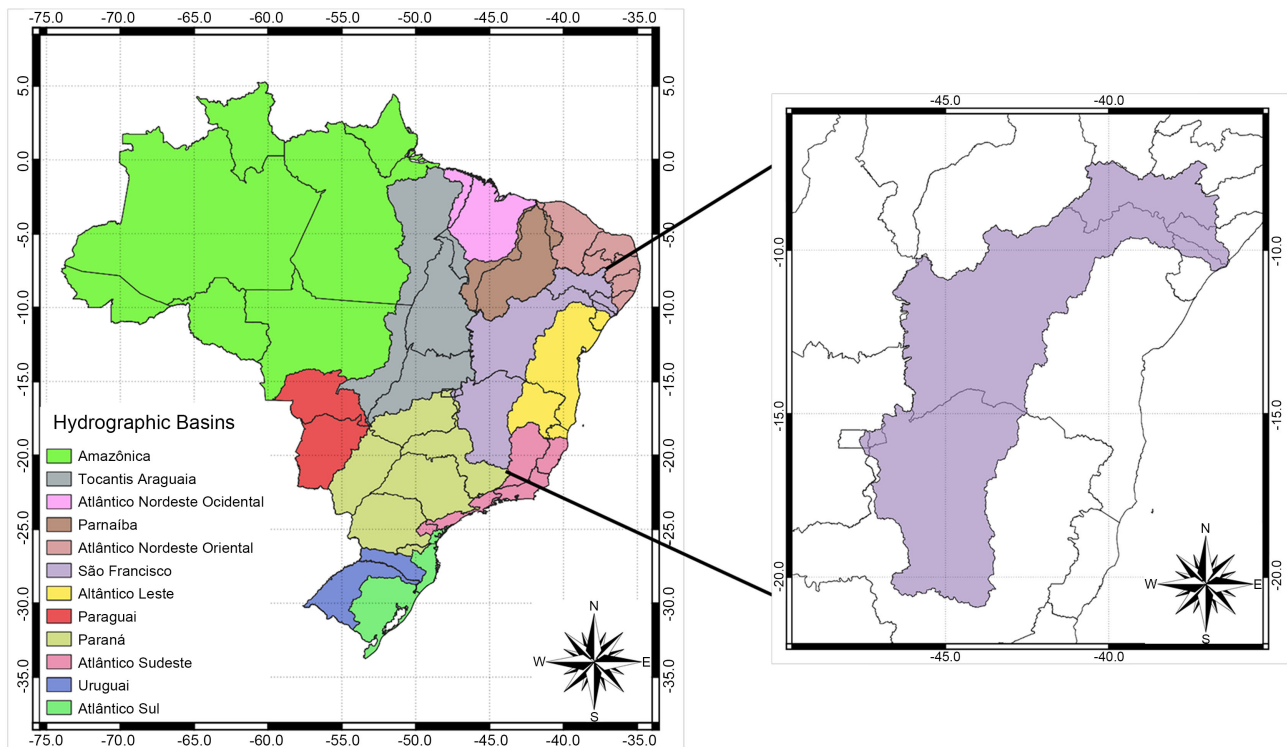


**Figure 1.** Map of the main watersheds in Brazil (left) as well as the SFRB (right). Colors indicate the watershed area. State boundaries, latitudes, longitudes are also indicated. Source: Author, 2022.

Northeast and Southeast Regions. It covers the east of the Federal District and the states of the northwest center of Minas Gerais, west of Bahia, west central Pernambuco, west center of Alagoas and north of Sergipe. It is divided into high São Francisco (Minas Gerais), middle São Francisco (between Minas Gerais and Bahia), Sub-middle São Francisco (Bahia, Pernambuco and Alagoas) and low São Francisco (Pernambuco, Alagoas and Sergipe) [14] [15].

The production of rainfall in this region comes from the South Atlantic Convergence Zone (SACZ), Frontal Systems (FS), Wave Disturbances of Tradewinds, South Atlantic Subtropical High, sea and land breezes [13] [16]. The SFRB is heterogeneous with four climatic types; at the headwaters, there is the tropical altitude, in the central region between Minas Gerais and Bahia the tropical type, between the north of Bahia and east of Sergipe and Alagoas the semi-arid and at the mouth the humid coastal type [17] [18].

## 2.2. Database

The precipitation data series of the National Water Agency (ANA) for SFRB was used in this research and the main oceanic indexes such as the Pacific Decadal Oscillation (PDO), Niño Ocean Index (NOI), Atlantic Multidecadal Oscillation (AMO), North Atlantic Oscillation (NAO) and the Atlantic Dipole (AD) and the number of sunspots in the period between 1950 and 2015, or 65-year monthly data series.

The above climate indexes time series are available from the Earth System Re-

search Laboratory (ESRL) of the Physical Science Division (PSD) of the National Oceanic and Atmospheric Administration (NOAA) and the sunspot number time series are available from the National Geophysical Data Center (NGCD) of the NOAA.

### 2.3. Precipitation Data Quality Control

ANA's precipitation database comprises 10,637 rain gauges in the entire Brazil. Precipitation data quality is a challenge since many precipitation time series lack consistency, have missing data, and are short in length. Furthermore, the rain gauge network is not evenly distributed as shown in **Figure 2(a)** as in [18]. The rain gauge network is sparse in Northern Brazil, especially in the Amazon, and denser in parts of Northeast (Ceará State) to and South (Paraná State) and Southeast (São Paulo and Rio de Janeiro States). Thus, the whole ANA precipitation database passed through a statistical data control procedure that reduced the time series to 3427 time series with the spatial distribution shown in **Figure 2(b)**. The selected time series begin in 1951.

Missing precipitation data is a cumbersome problem [19]. [20] used data filling methods such as regression equations with the least square adjustment for all-season available information and the regionally weighted method that is based on weighted averages of three or more neighbor rain gauge time series. This latter method yielded better results and corroborates with [21]. This latter method was used to fill missing precipitation data by using three neighbors ( $n = 3$ )

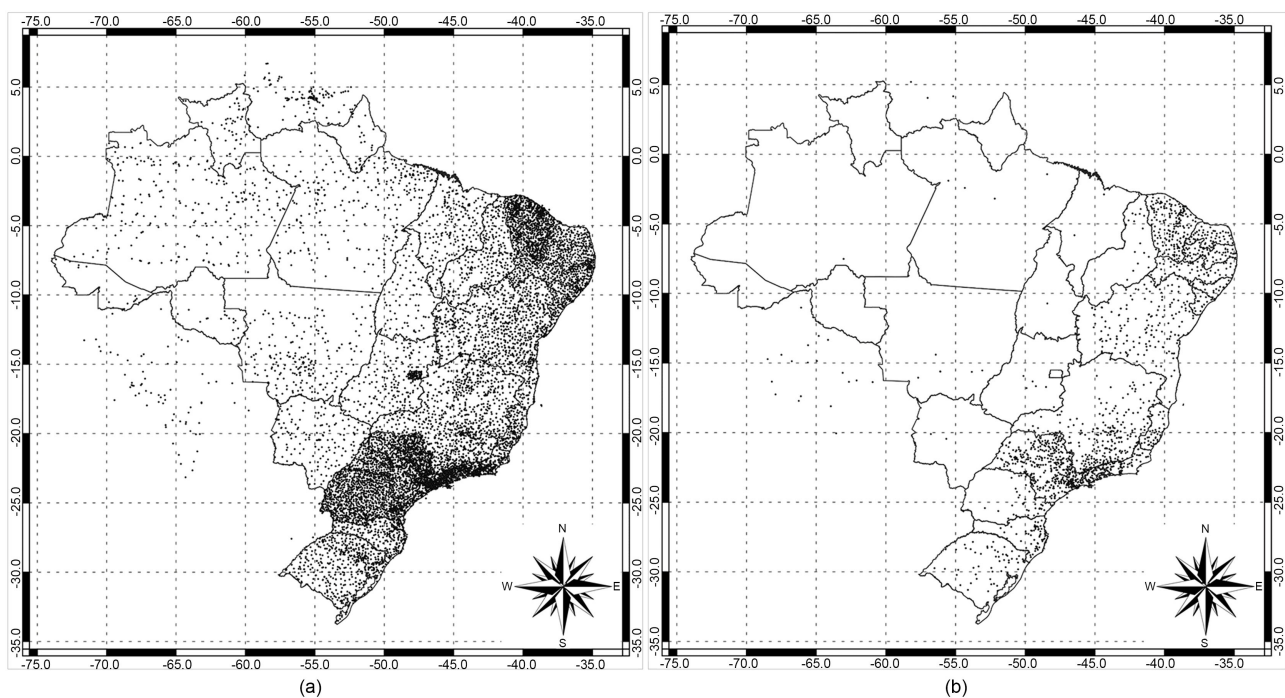


**Figure 2.** (a) Geographical location of the ANA precipitation network indicated by dots. (b) The geographic location of the precipitation network after the data quality control. Geopolitical boundaries, latitudes, and longitudes are indicated. Source: Author, 2022.

rain gauge time series for monthly and annual accumulations of time series longer than 10 years. The equation is:

$$P_x = \frac{1}{n} \sum_{i=1}^n \frac{Pm_x P_i}{Pm_i} \quad (1)$$

where,

$P_x$  is the precipitation estimation for the missing monthly data;

$P_i$  is the precipitation of the  $i^{\text{th}}$  neighboring rain gauge;

$Pm_{x(i)}$  is the long-term time average of the  $x(i)$  precipitation time series.

## 2.4. Cluster Analysis

Cluster analysis classifies individuals that participate in the same group given their similar characteristics or homogeneity. Individuals with similar analogies are classified as similar and those with heterogeneity are called dissimilar. To identify the similarity between individuals, it is quantified by the proximity of the similar and the dissimilar [22]. If the values are greater than zero, that is, the larger this number the more it will be similar and for values close to zero it will not be similar. And for dissimilar, it is the reverse, the higher the measured data, the less similar, and the smaller they are, the more similar [22]. So, cluster analysis separates data into groups whose identities are not known in advance. This more limited state of knowledge contrasts with the situation of discriminating methods that require a set of training data by which participation in the group is known. Cluster analysis is primarily an exploratory data analysis tool. Given a sample of  $x$  data vectors by defining the rows ( $n \times K$ ) of a data array  $[X]$ , the procedure will define groups and assign associations to groups at different aggregation levels [23].

## 2.5. Principal Component Analysis (PCA)

Pearson in 1901 started and Hotelling in 1933 expanded on PCA. It is a multivariate technique used to highlight and to identify variations in the dataset with strong patterns so to facilitate its interpretation and visualization [22] [24].

According to [23], this multivariate statistical technique is widely used in Meteorology. And it became popular by [25] who analyzed atmospheric data and gave the name of empirical orthogonal function analysis (EOF). PCA reduces a large number of variables time series into a fewer set of transformed variables. They are linear combinations of the original data and are chosen to represent the maximum possible fraction of the oscillation within the dataset. Although PCA is related to the multivariate statistical method, it is not a factor analysis since PCA uses all variables and the factor analysis explains all correlations using a few latent variables [22] [23].

## 2.6. Precipitation Anomaly

Precipitation anomaly is defined as the deviation from the long-term annual precipitation average:

$$A = P_i - P_m \tag{2}$$

where,

$A$  is the precipitation anomaly;

$P_i$  is the monthly precipitation;

$P_m$  is the long-term precipitation average for the month  $i$ .

The anomaly indicates the variability and extreme fluctuations in a given time series with marked deviations outside the observed sample of meteorological buoyancy [26]. It highlights the variability of precipitation regimes at different time scales and the analysis of cycles that change it [27].

### 2.7. Cross-Wavelet Analysis

The cross-wavelet transform (OCD) analyzes similarities and correlations among time series of variables to identify possible incoherence (out of phase) [28] [29] [30] [31]. The OCD analyzes periodic and non-stationary two-time series that might be related. It is based on the wavelet transform [32]. The OCD analysis plays an important role in comparing the frequency content of two-time series to determine periodicities and respective time intervals. The phase of the time series is analyzed through the position of arrows displayed on a cross-point powers spectrum diagram [33] as shown in **Figure 3**. According to [33] [34], OCD can be compared to the covariance between two variables, but it depends on their measurement units which can difficult the analysis. Thus, the consistency of wavelets facilitates the analysis. The relationship between the two-time series is obtained from the coherence of wavelets. The axis of the abscissa (ordinate) represents the time (time scale), a color scale represents the magnitude of the variation coefficient  $R^2$ , the white line indicates areas of significant coherence, the arrows indicate the relationship between the time series.

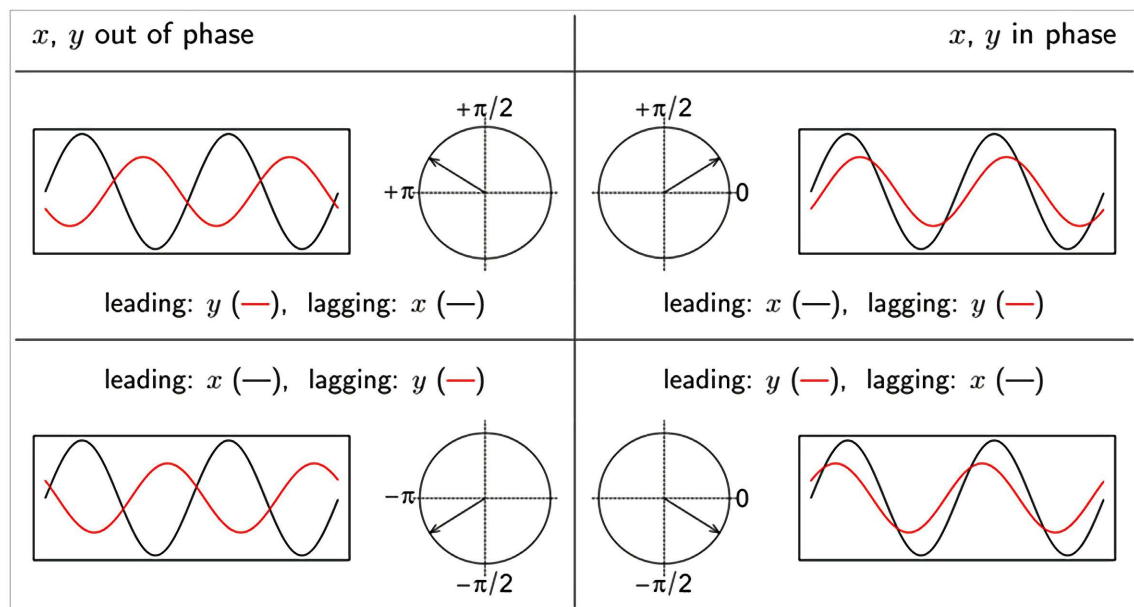


**Figure 3.** Phase difference and its interpretation. From [34].

The relationship between phases is given by the arrows in the OCD diagram. **Figure 3** shows a phase difference diagram. In (out) phase or positive (negative) correlation if the arrows are pointing to the right (left) and the position of the arrows in each quadrant indicates which time series is leading. A value of 0 means that cycles move together at certain periods [35] [36] [37]. A phase difference of  $\pm\pi$  indicates that time series cycles are shifted by  $180^\circ$ , *i.e.*, representing a perfectly negative correlation ( $y$  or  $x$  leading). The arrows pointing up mean that the  $y$  (or  $x$ ) time series is ahead of the second in  $90^\circ$ , while the down-pointing arrows indicate that  $x$  (or  $y$ ) of the time series is ahead of the first in  $90^\circ$  [35] [36] [37].

## 2.8. Boxplot

The boxplot diagram in **Figure 4** is a quantitative method of AED also known as schematic drawing defined by the first and third quartiles and by the median. For interpretation, there are two limits one lower and one higher, which is below or above these limits are called outliers, the median that is the central value [38].

The minimum, median and maximum values are the 1<sup>st</sup>, 2<sup>nd</sup>, and 3<sup>rd</sup> quartiles, representing 25%, 50%, and 75% of the dataset. The outliers are the extremes [39].

## 2.9. Standardized Precipitation Index

The Standardized Precipitation Index (SPI) is a widely used methodology to quantify droughts and rainfall extremes of a given study area. [40] analyzed the normalized monthly precipitation data using the probability distribution function that describes the time series. **Table 1** shows SPI values for wet (positive) and dry (negative) conditions. Drought and floods begin at  $SPI = 1$  and  $SPI = -1$ , respectively.  $SPI$  lower than  $|1|$  indicates normal conditions [31] [41] [42].

According to the European Drought Observatory [43], the SPI is used for detecting and distinguishing drought conditions. The precipitation anomaly for a

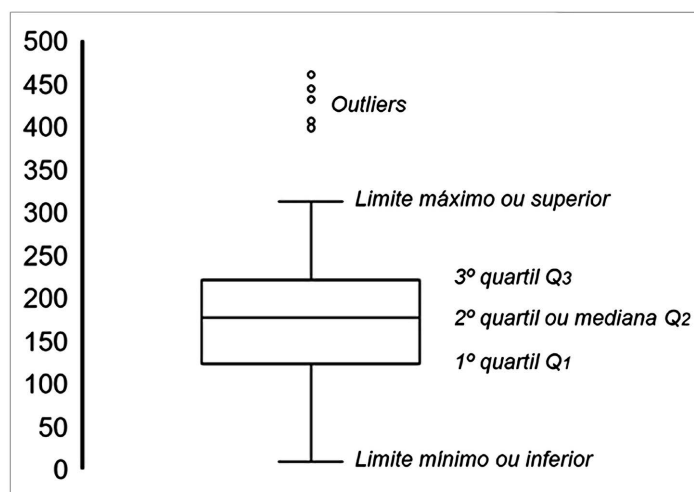


**Figure 4.** Schematic of a boxplot diagram. Source: Author, 2022.

**Table 1.** Values of the standardized index of precipitation and classes of drought and humidity. Source: McKee *et al.* [40].

Standardized Precipitation Index	Condition
$\geq 2.00$	Extremely Humid
1.50 a 1.99	Severely Humid
1.00 a 1.49	Moderately Humid
0.00 a 0.99	Initial Humidity
0.00 a -0.99	Initial Dry
-1.00 a -1.49	Moderately Dry
-1.50 a -1.99	Severely Dry
$\leq -2.00$	Extremely Dry

given precipitation accumulation time interval, for instance, 1, 3, or 12 months is equivalent to SPI-1, SPI-3, and SPI-12, respectively. A seven-month accumulation time interval was used in this study.

### 3. Results and Discussion

#### Precipitation Analysis in the São Francisco River Basin

**Figure 5** shows the location of the 199 rain gauge time series selected within the SFRB to perform a diagnostic statistical. **Figure 6** shows the spatial-temporal long-term monthly precipitation average and respective standard deviation for the SFRB between 1950 and 2015. The average and standard deviation indicate a well-defined annual cycle with wet and dry periods. The amplitude of standard deviation is in phase with the average precipitation. The SFRB precipitation regime is affected by FS, SAZS, sea and land breezes, and isolated [17].

The SFRB is slightly drier with a high amplitude standard deviation. Upstream the SFRB, the precipitation regime is influenced by the SACZ and, downstream, by the South Atlantic Subtropical High (SAHPS) that suppresses precipitation though close to the SFRB outlet, sea breezes increase the precipitation [17]. The weather systems over the SFRB are under the two major precipitating regimes of the southeast (wetter) and northeast (drier). In the upper SFRB in Minas Gerais State (**Figure 1**), the weather systems are associated with SAZC, FS, LI, CCM, and isolated convection. The middle SFRB area is in between northwest of Minas Gerais State and western Bahia State, SAHPS and Upper Tropospheric Cyclonic Vortex (UTCV) area major weather systems. The sub-middle SFRB is in between the north of Bahia State, west of Pernambuco State, and the extreme west of Alagoas State (**Figure 1**), SAHPS, UTCV, ITCZ, and, LI are the main weather systems affecting the precipitation regime. Finally, the lower SFRB in between Pernambuco State, Bahia State, Alagoas State, and Sergipe State, is affected by the types of weather systems on its mid-area and easterlies wave disturbances and sea and land breezes [13] [17].

**Figure 7** shows the average annual precipitation in the SFRB. In extremely dry



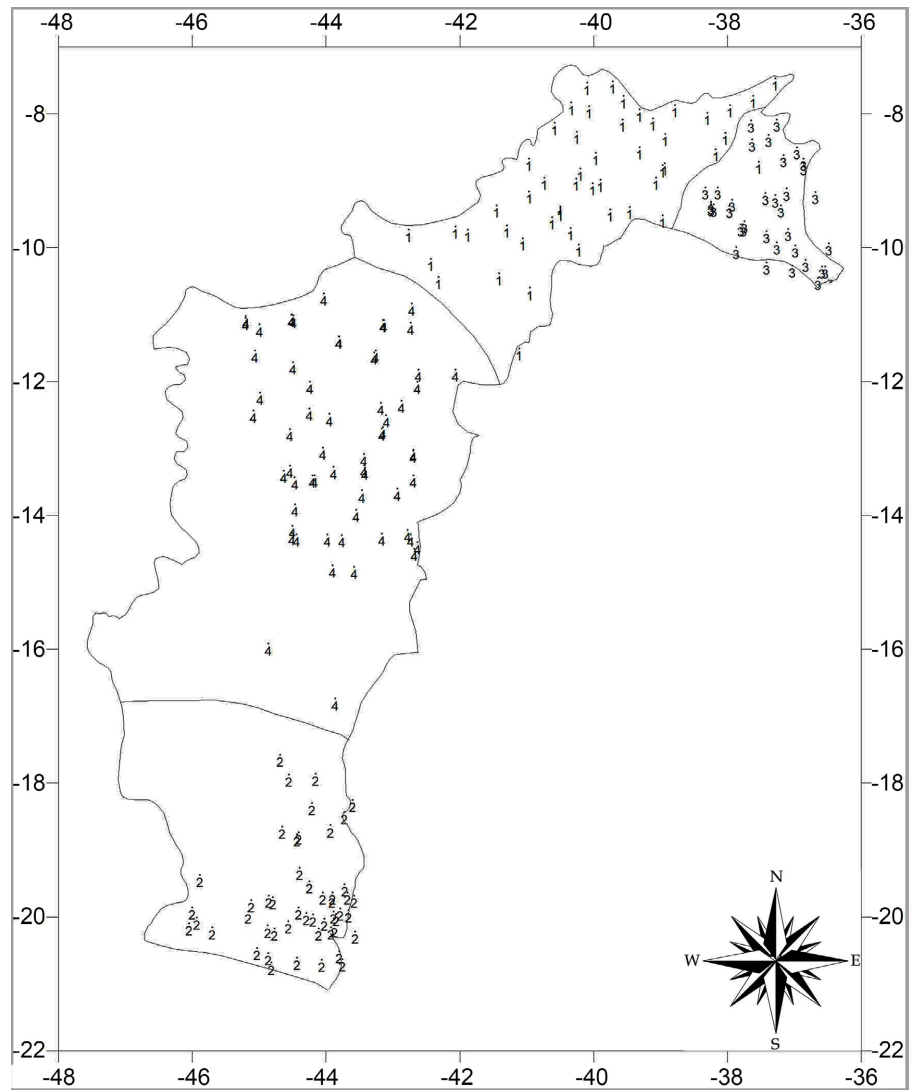


**Figure 5.** Distribution of the 199 rainfall stations in the São Francisco River Basin. Source: Author, 2022.

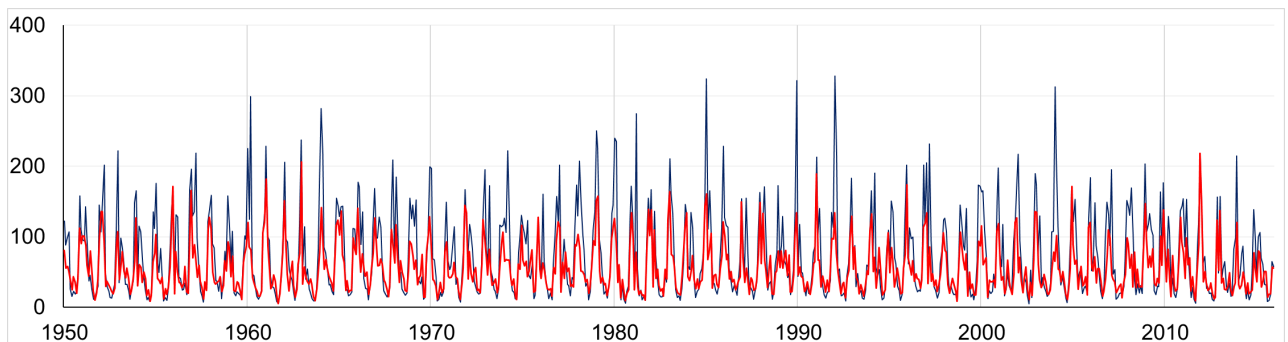


**Figure 6.** Temporal evolution of the spatial-temporal monthly precipitation average (blue line) and respective standard deviation (red line) for the SFRB between 1950 and 2015. Source: Author, 2022.

years, the annual precipitation was <700 mm. It was 652.9 mm in 1959 under a weak El Niño (EN), 625.7 mm in 1963 (moderate EN), 593.7 mm in 1990 (neutral),

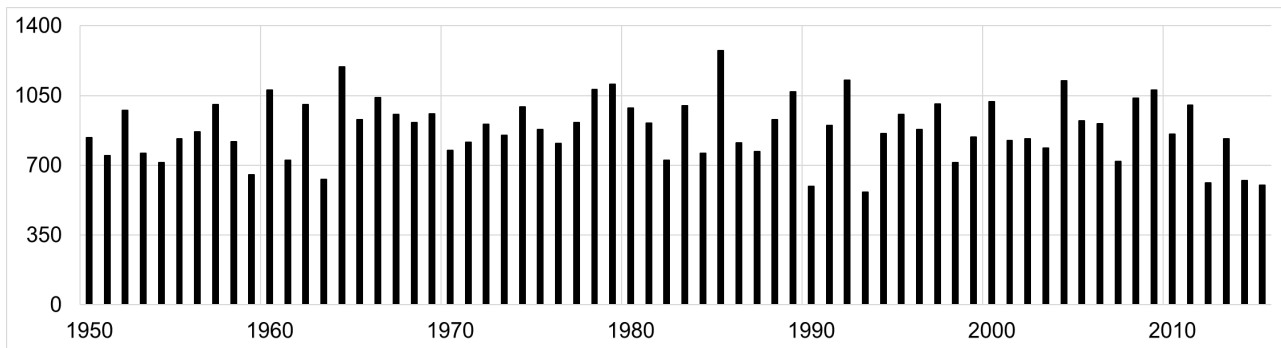


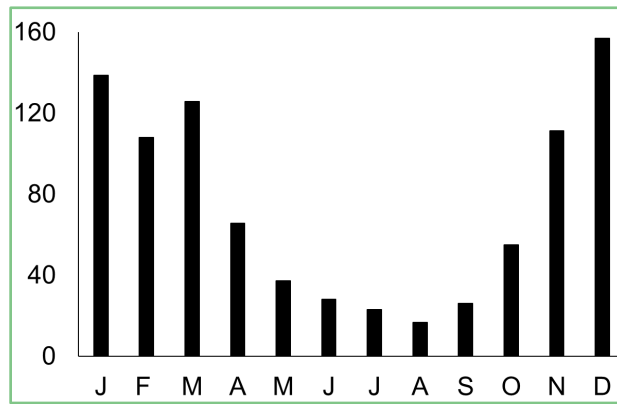
**Figure 7.** Temporal evolution of the spatial annual precipitation average for the SFRB between 1950 and 2015. Source: Author, 2022.

566.2 mm in 1993 (neutral), 612.6 mm in 2012 (weak LN), 625.3 mm in 2014 (neutral) and 601.8 mm in 2015 (very strong EN). On the other hand, in extremely wet years, the annual precipitation was >1000 mm. It was 1004.7 mm in 1957 (strong EN), 1079.3 mm in 1960 (neutral), 1004.6 mm in 1962 (neutral), 1195.3 mm in 1964 (weak La Niña (LN)), 1039.1 mm in 1966 (EN forte), 1082.0 mm in 1978 (weak EN), 1108.2 mm in 1979 (weak EN), 1274.7 mm in 1985 (weak LN), 169.8 mm in 1989 (strong LN), 1126.1 mm in 1992 (moderate EN), 1007.7 mm in 1997 (very strong EN), 1018.4 mm in 2000 (moderate LN), 1124.0 mm in 2004 (weak EN), 1038.1 mm in 2008 (moderate LN), 1077.1 mm in 2009 (moderate EN) and 1002.5 mm in 2011 (moderate LN).

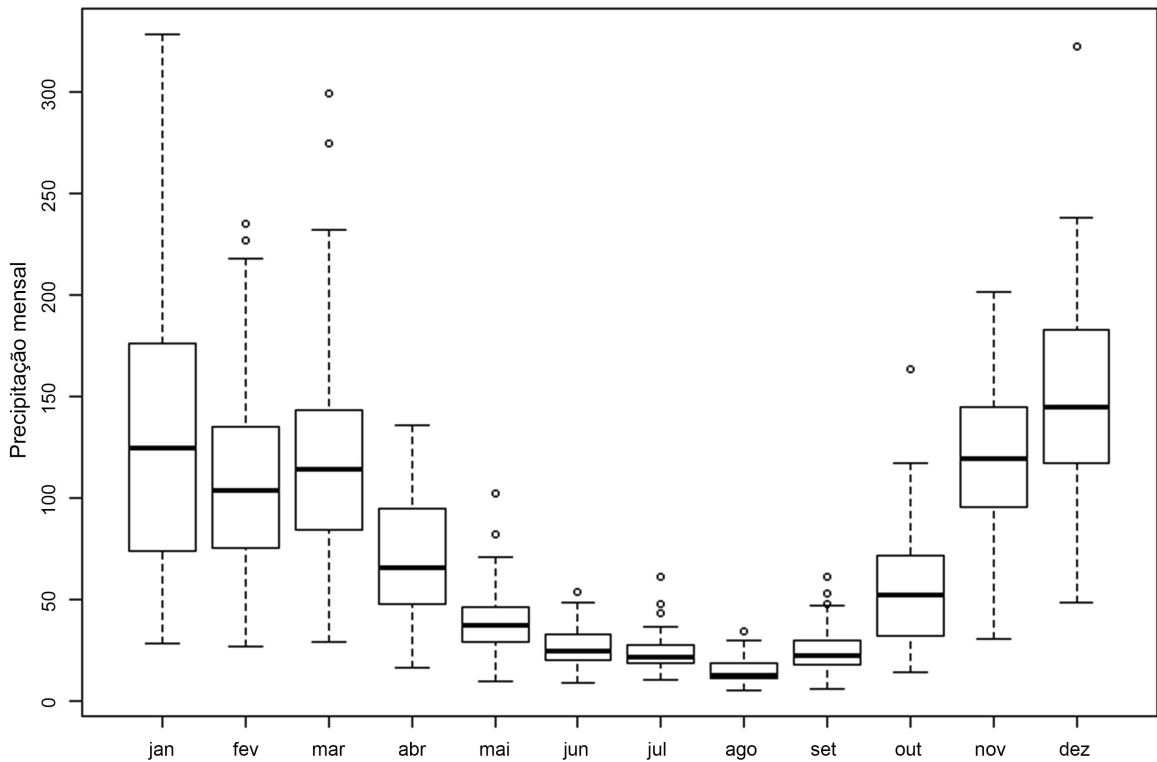
The monthly precipitation climatology for the SFRB between 1981 and 2010 is shown in **Figure 8(a)**. The average annual cycle is irregular given the increase of the precipitation in March during the transition between summer and fall when the monthly precipitation diminishes in the upper SFRB and increased downstream. **Figure 8(b)** shows the boxplot for the precipitation climatology between 1950 and 2015. A great spatial-temporal variability occurs during the rainy season from November to March. For instance, in January, the minimum and maximum are 28.3 mm and 328.3 mm, respectively. It is greatly reduced between May and September. For example, in August, it varies between 5.3 mm and 33.9 mm.

**Figure 9** shows the temporal evolution of annual and monthly SPIs for the SFRB between 1950 and 2015. **Figure 9(a)** shows that there is great variability between very wet and very dry periods. Between 1962 and 1964 there was high precipitation. In contrast, in 1961 occurred a moderate drought. Similarly, between 1979 and 1982 there was a drought. **Figure 9(b)** and **Figure 8** show a dry period between April and October and, a wet one, between November and March. Noteworthy, no precipitation occurred for almost the entire year between 1970 and 1972 but November and December.

**Figure 10** shows the monthly frequencies of SPI for the SFRB between 1950 and 2015. There is an initial drought (November, January, February, and March) in the rainy months as well as high wet conditions initial in April. The SPI is then reduced in the next few months until August with the highest frequency of droughts even extreme ones.

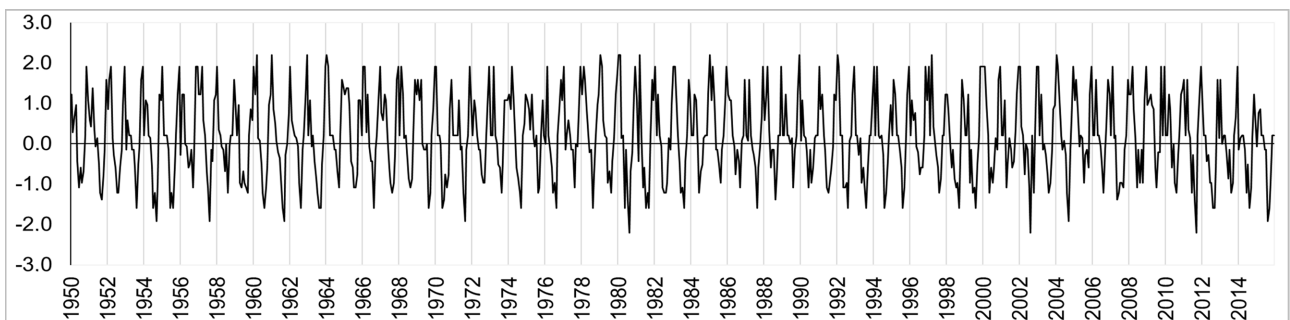


(a)



(b)

**Figure 8.** The SFRB long-term spatial-temporal precipitation average (mm) for 199 rain gauges time series between 1981 and 2010 (a) and the boxplot for 1950 to 2015 (b). Source: Author, 2022.



(a)

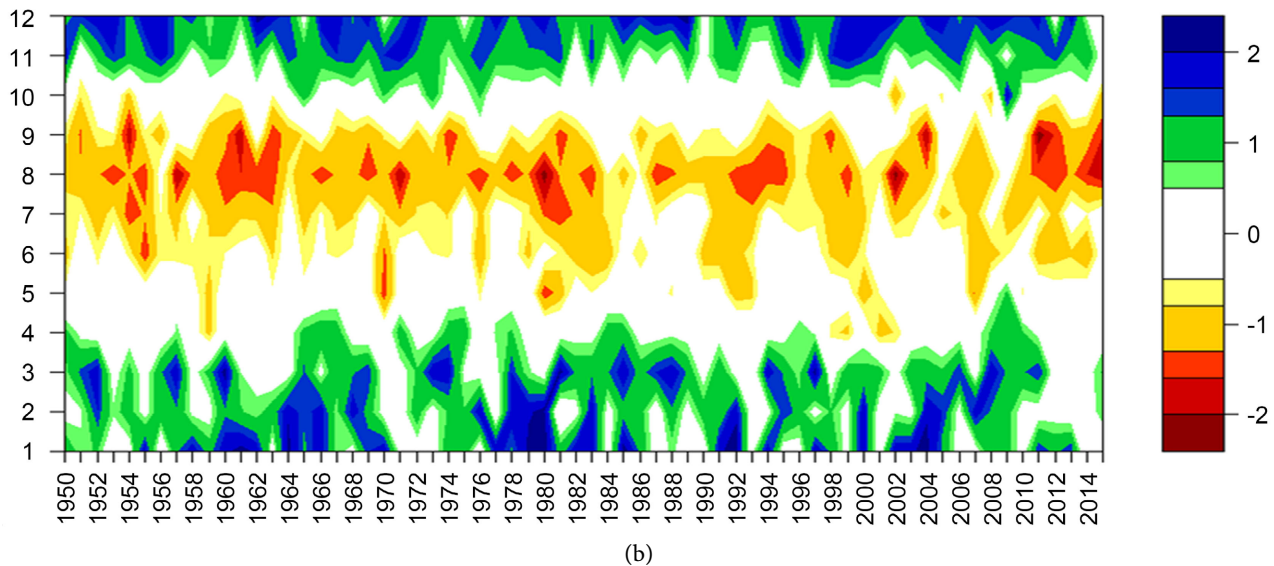


**Figure 9.** Time evolution of annual (a) and monthly (b) of SPI of the SFRB for 199 rain gauge time series between 1950 and 2015. Source: Author, 2022.

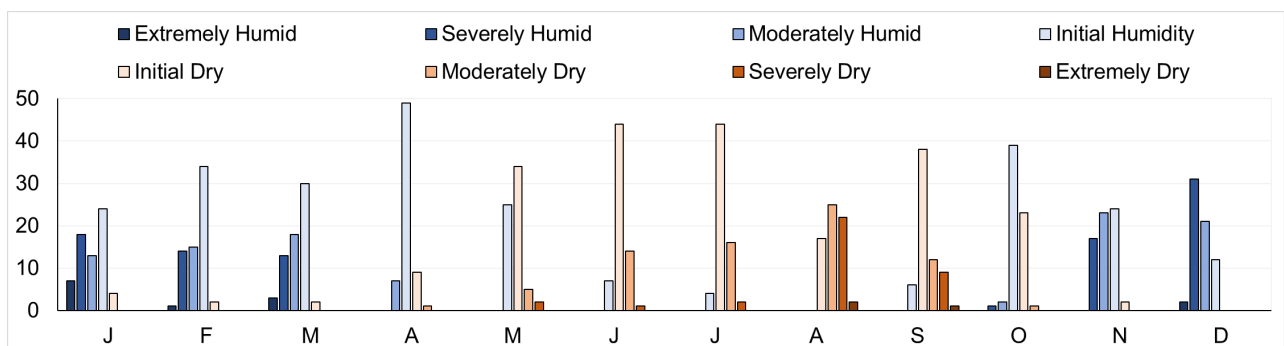


**Figure 10.** Monthly frequencies of the SPI index (Table 1) for the SFRB between 1950 and 2015. Source: Author, 2022.

**Figure 11** shows the spatial distribution of the annual average precipitation and the four homogeneous areas within SFRB from 1981 to 2010. **Figure 11(a)** indicates that along the FSRB the average annual precipitation varies between 1500 mm in upper SFRB and 500 mm in its sub-middle portion. In **Figure 11(b)**, the RH1 region corresponds to the lower São Francisco with 36 rain gauges and  $>600 \text{ mm}\cdot\text{yr}^{-1}$ . It is supplied with precipitation of sea and land breezes, and easterly waves disturbances systems. The RH2 region in the sub middle is the driest one in SFRB with 51 rain gauges and precipitation between  $500 \text{ mm}\cdot\text{yr}^{-1}$  and  $600 \text{ mm}\cdot\text{yr}^{-1}$  from EWP, UTCV, FS, and SAZC weather systems. RH3 in middle SFRB has 63 rain gauges with annual precipitation between  $500 \text{ mm}\cdot\text{yr}^{-1}$  and  $1000 \text{ mm}\cdot\text{yr}^{-1}$  500 to 1000 mm/year. It is the most heterogeneous area. There are 49 rain gauges in RH4 with an annual precipitation average  $> 1400 \text{ mm}\cdot\text{yr}^{-1}$ . The major precipitating systems in RH 3 and RH4 are UTCV, SF, SAZC, CCM, LLJ, and SAHPS.

**Figure 12** shows the boxplots for the monthly average precipitation time series for each of the four homogeneous regions (**Figure 11(b)**). These statistics

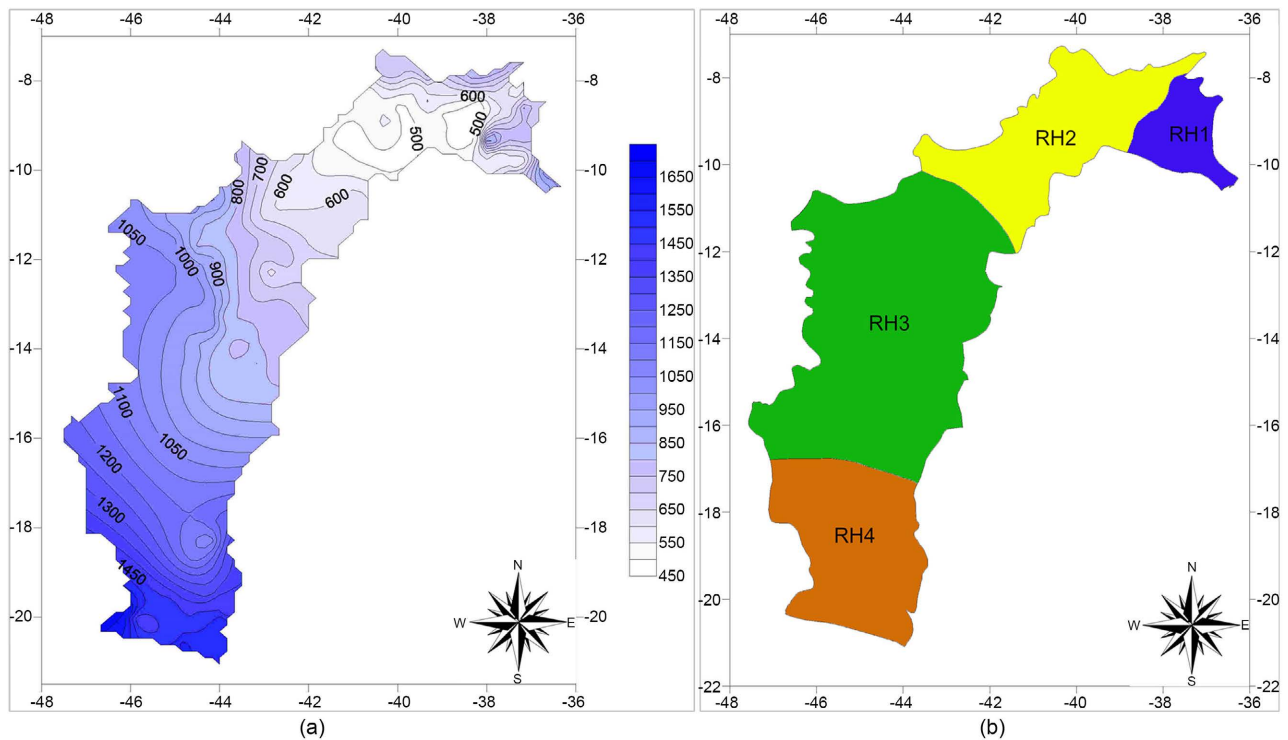


**Figure 11.** Spatial distribution of the annual average of precipitation (a) and the classification of homogeneous precipitation regions of ward's clustering method to the main spatial common factors of the precipitation average of the 199 stations of the SFRB between 1980 and 2010 (b). Source: Author, 2022.

indicate large fluctuations in the four regions over the years. The boxplot for RH1 (Figure 12(a)) presented outliers between June and April. May is the wettest but without outliers. The lowest monthly average precipitation occurs in the dry season in regions RH2, RH3, and RH4 shown in Figures 12(b)-(d) and outliers during the dry and wet seasons. The RH1 region covers an area of 32,013 km<sup>2</sup> with a river length of 208 km [44]. The monthly average precipitation in RH1 (Figure 12(a)) is higher in March, April, July, and August and lower in September, October, January, and February ranging from 24 mm to 99 mm. The RH2 region covers an area of 155,637 km<sup>2</sup>, with a river length of 42 km [44]. The average monthly precipitation (Figure 12(b)) is distinct from RH1 with the highest precipitation between December and April and the lowest between May and November. The RH3 region covers an area of 337,763 km<sup>2</sup> with a river length of 1300 km [44]. The average monthly precipitation is highest between November and March, and the lowest from April to October (Figure 12(c)). Finally, the RH4 region covers an area of 111,804 km<sup>2</sup> [44]. The average monthly precipitation is similar to the RH3 region (Figure 12(d)).

Figure 13 shows the evolution of the monthly precipitation anomalies of the four homogeneous regions in the SFRB from 1950 to 2015. Anomalies in the RH1 region are low in amplitude during wet months, except for the positive ones in 1957, 1960, 1963, 1966, 1975, 1981, 1985, 1992, 1994, 1996, 2002, 2004, and 2009, with their respective monthly average precipitation of 180 mm, 276 mm, 158

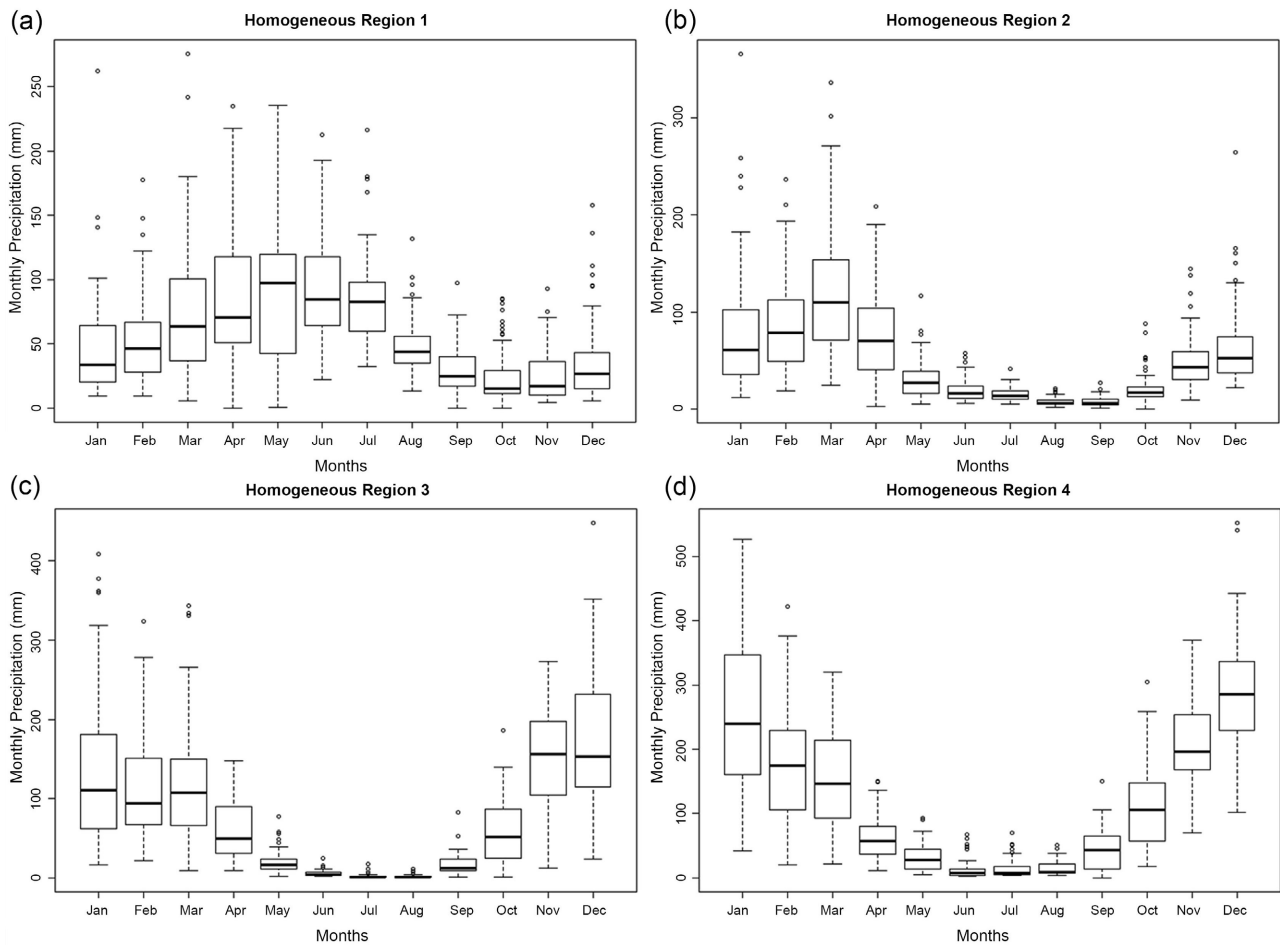


**Figure 12.** Boxplots of the monthly average precipitation (1981-2020) for RH1 (a), RH2 (b), RH3 (c), and RH4 (d) in the SFRB. Source: Author, 2022.

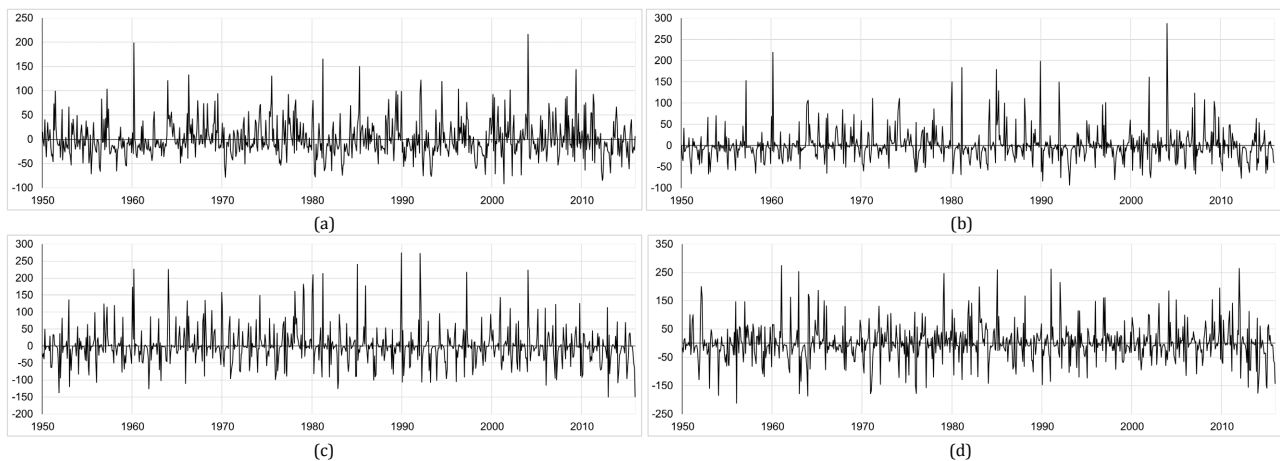


**Figure 13.** Time evolution of the monthly precipitation anomalies in the SFRB between 1950 and 2015 for the homogenous regions (Figure 11(b)) RH1 (a) RH2 (b), RH3 (c), and RH4 (d). Source: Author, 2022.

mm, 217 mm, 216 mm, 242 mm, 235 mm, 177 mm, 212 mm, 188 mm, 148 mm, 262 mm and 235 mm. All of them but 1963, 2002, and 2004 in the dry season

(December and January). Significant negative anomalies occurred in the wet season in April, May, and June in 1955, 1970, 1980, 1983, 1992, 1993, 1999, 2000, 2001, 2002, 2003, 2012 with respective monthly precipitation of 22 mm, 14 mm, 14 mm, 17 mm, 16 mm, 8 mm, 12 mm, 20 mm, 0.2 mm, 9 mm, 11 mm and 0.0 mm. In the RH2 region (**Figure 13(b)**) the negative anomalies are less variable while larger positive anomalies occurred in 1957, 1960, 1980, 1981, 1985, 1989, 1992, 2002, and 2004, with 271 mm, 337 mm, 237 mm, 302 mm, 258 mm, 264 mm, 229 mm, 240 mm and 366 mm, respectively. More significant negative anomalies occurred in 1990 (34 mm), 1992 (42 mm), 1993 (25 mm), 1998 (37 mm), 2002 (42 mm), and 2012 (2 mm) in March, the wettest month except in 2012 that occurred in April. A greater variability between positive and negative anomalies is observed in the RH3 region (**Figure 13(c)**) with positive ones in 1960 (January), 1960 (March), 1964, 1969, 1974, 1978, 1979, 1980, 1981, 1985 (January), 1985 (December), 1989 1992, 1997 and 2004, with respective precipitation of 310 mm, 343 mm, 362 mm, 332 mm, 266 mm, 274 mm, 319 mm, 323 mm, 330 mm, 377 mm, 351 mm, 448 mm, 408 mm, 334 mm and 360 mm. The major negative anomalies in the wet season occurred in 1951, 1953, 1961, 1982, 2006, 2012, and 2015 with precipitation of 13 mm, 17 mm, 23 mm, 24 mm, 21 mm, 24 mm, and 24 mm, respectively. Finally, positive anomalies in the RH4 region (**Figure 13(d)**) were observed within the wet season except in 2009 with significant precipitation in the transition period (October). The most significant positive anomalies occurred in 1952 (376 mm), 1961 (527 mm), 1962 (541 mm), 1979 (423 mm), 1983 (452 mm), 1985 (266 mm), 1991 (515 mm), 1992 (467 mm), 2004 (361 mm), 2009 (304 mm) and 2011 (552mm). And the most significant negative anomalies that occurred in the wet season were in 1953, 1954, 1956, 1963, 1963, 1970, 1976, 1977, 2012, 2014, and 2015 with precipitation of 94 mm, 69 mm, 42 mm, 75 mm, 101 mm, 110 mm, 75 mm, 20 mm, 133 mm, 76 mm and 95 mm, respectively. All these negative rain anomalies occurred in the rainy season.

The cluster analysis used to identify the four homogenous regions (**Figure 11(b)**) yielded eight common factors shown in **Table 2** that explained 91.2% of the total variance of the data, though the first 4 factors were explained 87.4% of the monthly average precipitation of the 199 rain gauges precipitation time series. They were used to determine the homogenous regions in the SFRB.

The spatial patterns associated with the first four factors of **Table 2** for each homogeneous region are shown in **Figure 14**. They define the spatial patterns of precipitation in the SFRB. The spatial pattern of the first PC explained 28.0% of the variance of the monthly precipitation average. The highest first factor (0.8) is in the central part of the SFRB collocated to the highest precipitation. This precipitation pattern is caused by mountain valley breezes, SAZCs, and FSs with the dry pre-season from May to September and with the wet season between November and April, given the prevailing precipitating systems in this region. The second principal component explained 27.0% of the variance of the monthly

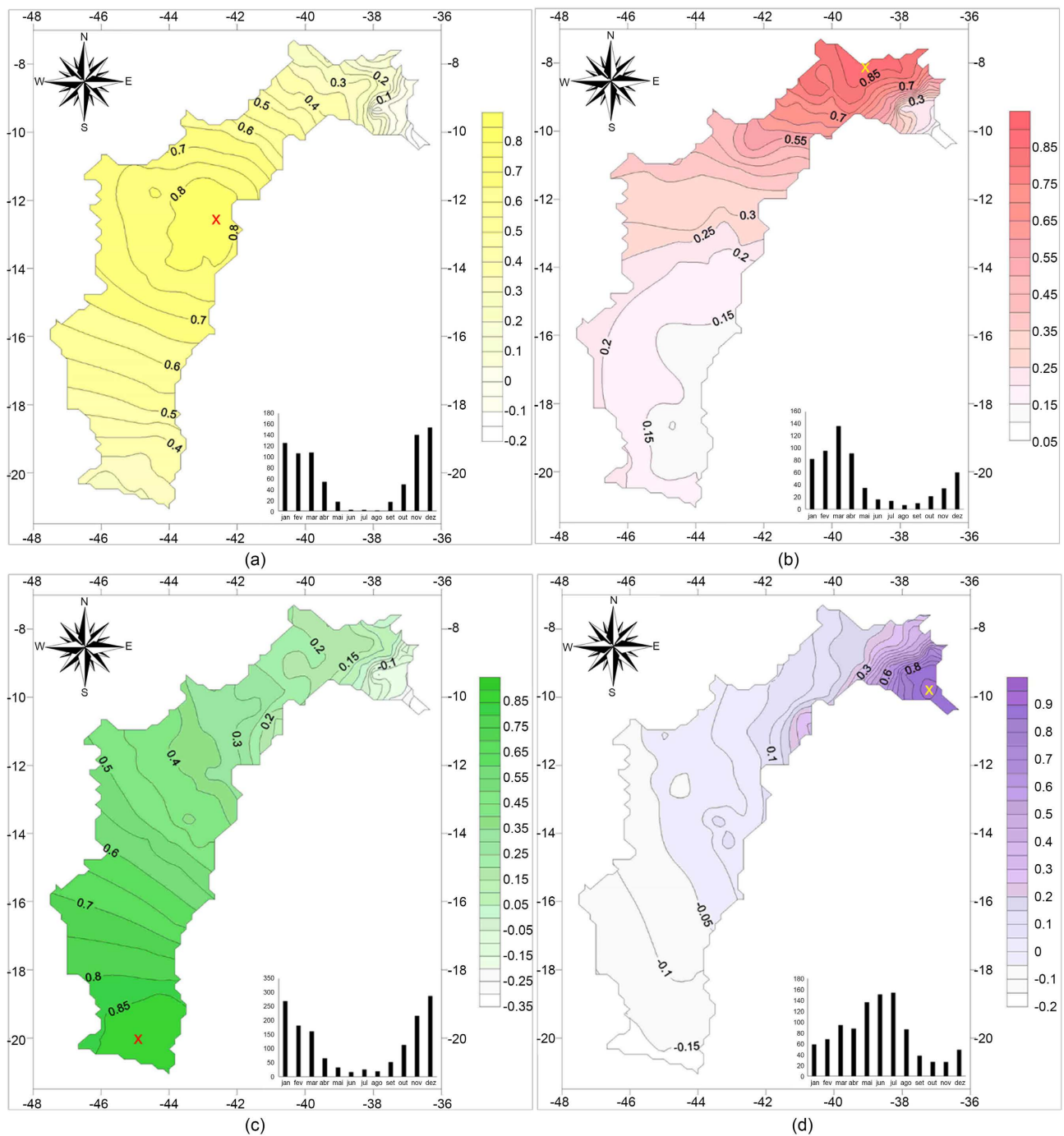


**Figure 14.** Spatial distribution of the first (a), second (b), third (c), and fourth (d) temporal factors (Table 2) for the SFRB. Latitudes, longitudes, color scales are indicated as well as the precipitation for each factor. Source: Author, 2022.

precipitation average with higher values upstream the SFRB, reaching above 0.8. It might be related to SAZCs, local convection, and FSs. The wet and dry season patterns are similar to that of the first PC. The third PC explained 21.0% of the variance of the monthly precipitation average and with exceeding a maximum greater than 0.8 was downstream the SFRB where the ITCZ, squall lines, and UTCV common precipitation producing systems during the wet season from



**Table 2.** Eigenvalues and total variance for the monthly precipitation average of in the SFRB. Source: Author, 2022.

Principal Component	Non-rotated factors			Rotated factors		
	Eigenvalue	Explained Variance (%)	Accumulated Variance (%)	Eigenvalue	Explained Variance (%)	Accumulated Variance (%)
1	115.275	57.927	57.927	55.515	27.897	27.897
2	41.428	20.818	78.745	52.524	26.394	54.291
3	9.231	4.639	83.384	41.670	20.940	75.231
4	8.878	4.461	87.845	24.247	12.185	87.415
5	2.534	1.273	89.118	2.426	1.219	88.635
6	1.706	0.857	89.976	2.069	1.040	89.674
7	1.318	0.662	90.638	1.688	0.848	90.522
8	1.099	0.552	91.190	1.328	0.667	91.190
...	...	...	...	...	...	...
199	...	...	100	...	...	100

January to April. Finally, the fourth PC explained 12.2% of the variance of the monthly precipitation average rain with contributions exceeding 0.8 in the lower SFRB where the wet season is between April and August, and the dry season between September and March. Noteworthy, the first two CP are associated with the wet season with precipitation from the Southeast region of Brazil while the last two PC correspond to the precipitation of the Northeast region of Brazil [45].

#### 4. Spectral Analysis of the SFRB

Spectral analyses between the monthly precipitation average anomalies of the entire SFRB and oceanic indices were obtained. **Figure 15** shows a panel with the time evolution of monthly precipitation average anomalies of the SFRB, cross-wavelet spectrum diagram, the global cross-wavelet spectrum, the time evolution of the Niño Ocean Index (NOI), and the precipitation monthly average climatology for the period from 1950 to 2015. The relationship between precipitation anomalies and the Niño Ocean Index (NOI) in the cross-wavelet (**Figure 15(b)** and **Figure 15(c)**) indicates that the high-power cores have periodicities of 1.5, 2, and 4 years and a secondary one at 11-year cycle. Between 1950 and 1960, there are three high power cores at 1.5 and 3 to 7 years, 8 to 11 years, and >16 years. The 1.5-year core at the end of the 1950s shows two signs, one where the NOI leads over the precipitation in opposite phase or negative NOI and another sign that the series move opposite with perfectly negative correlation (**Figure 15(d)**). The core centered between 3 and 7 years indicates that the precipitation anomaly leads the NOI or the precipitation anomaly occurs 3-months before the NOI. But at the beginning of the 60s, the NOI led over the

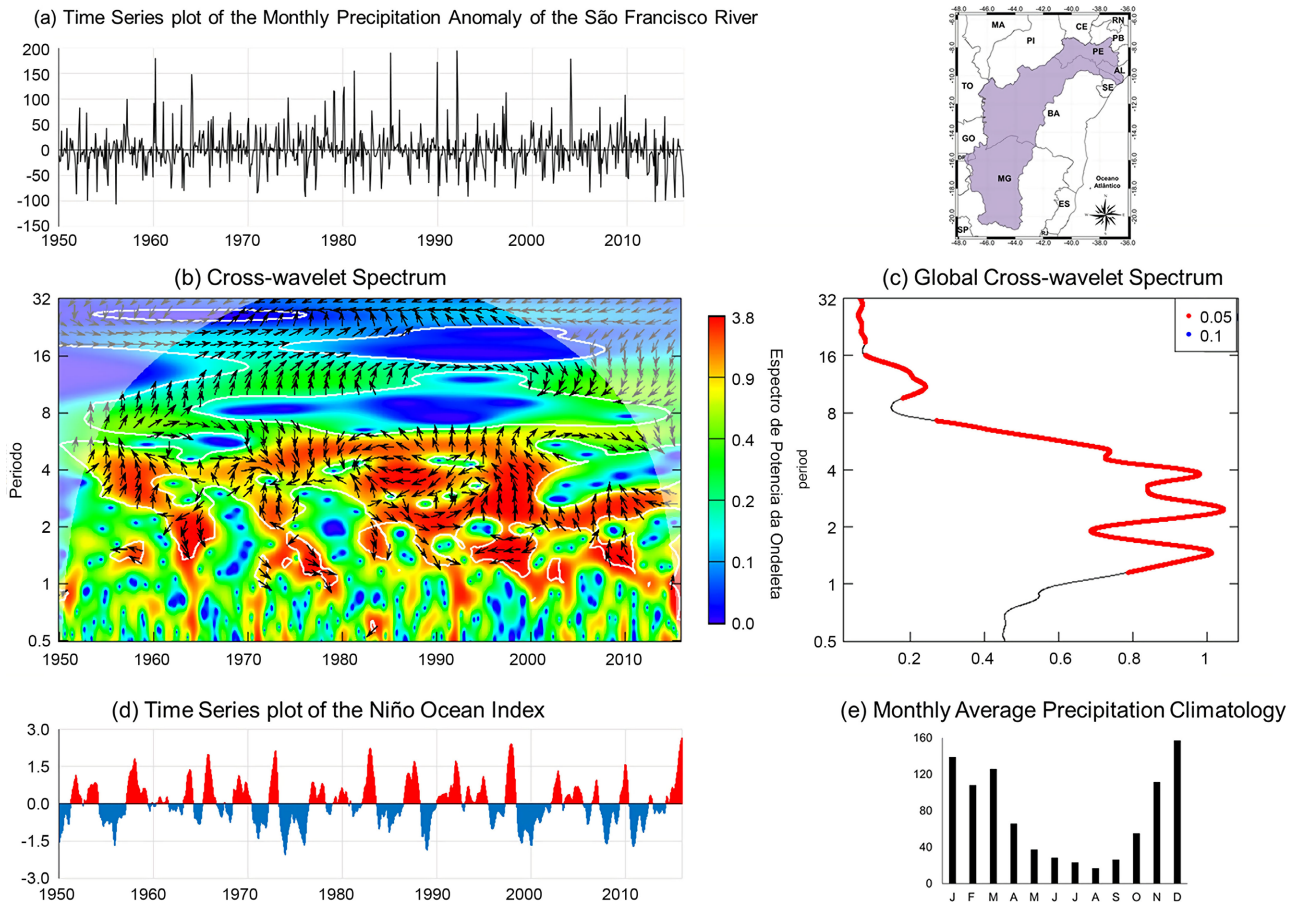


**Figure 15.** Time evolution of monthly precipitation average anomalies of the SFRB (a), cross-wavelet spectrum diagram (b) and respective global cross-wavelet spectrum (c), the time evolution of the Niño Ocean Index (NOI) (d), and the precipitation monthly average climatology for the period from 1950 to 2015. Source: Author, 2022.

precipitation anomaly (negative correlation) with a time response of 4.5 months near the end of the 60s. Between the 60s and 70s, the high-power core between 1.5 and 3 years, the anomalies are out of phase close to 2-years. So, the precipitation led on NOI, as it approached the 3-year range move together, and on the 3-year time scale, the NOI led the precipitation. On the 7-year time scale, both move along with correlation perfectly positive. As it approached the 70s, the NOI was 45 deg ahead of precipitation or about 1.5 months. The NOI showed more positive anomalies than negative ones in the entire period. Between the 70s and 80s, 1-year and 2-year timescales, the positive NOI led. Conversely, the precipitation led to the negative NOI. Between 2-year and 4-year time scales, practically the precipitation led over the NOI during negative anomalies starting at the 4-year time scale, while the NOI led the precipitation with a 3-months response. In the 80s and late 90s, the spectral power was higher between 1-year and 7-years. In 1982 and 1983, the NOI was a positive anomaly, with a 6-months periodicity, the precipitation anomaly led over the NOI. And between 1-year and 2-year time scales, the NOI was ahead of the precipitation anomaly with a 3-month response. This response decreased to about 1.5 months until the early

90s. Between 1995 and 2001, the negative NOI, between 1-year and 2-year time scales moved opposite and from the 2-year time scale, the NOI is 90 deg out of phase with the precipitation anomaly. After 2004, practically, the precipitation led the NOI until 2010 when the ION returned to lead over the precipitation anomaly.

The most evident annual periodicity is shown in **Figure 16** from 2 years up to 32 years period with a 5% of statistical significance or 95% confidence. Between 1950 and 1960, there are two cores of high variability between 1-year and 2-year and 2-year to 11-year. The first core shows that when the PDO was negative, it led over the precipitation while when it was positive, both were in phase with the precipitation leading, and soon after, the PDO led over the precipitation. In the 2-year to 4 years cycles, the PDO and the precipitation are in phase, and as the cycle increases and approaches 4-years, the rain leads. As it approaches the 7-year cycle, the PDO leads the precipitation. But between 1980 and 2005, the anomaly series moved opposite to each other with a perfectly negative correlation. And between the 4-year and 8-year cycles, similar behavior was observed in the 50s and 60s.

**Figure 17** shows the most significant variability in the annual cycle but for the 2, 4, 7, 11, and 22-year cycles with a statistical significance of 95% confidence.

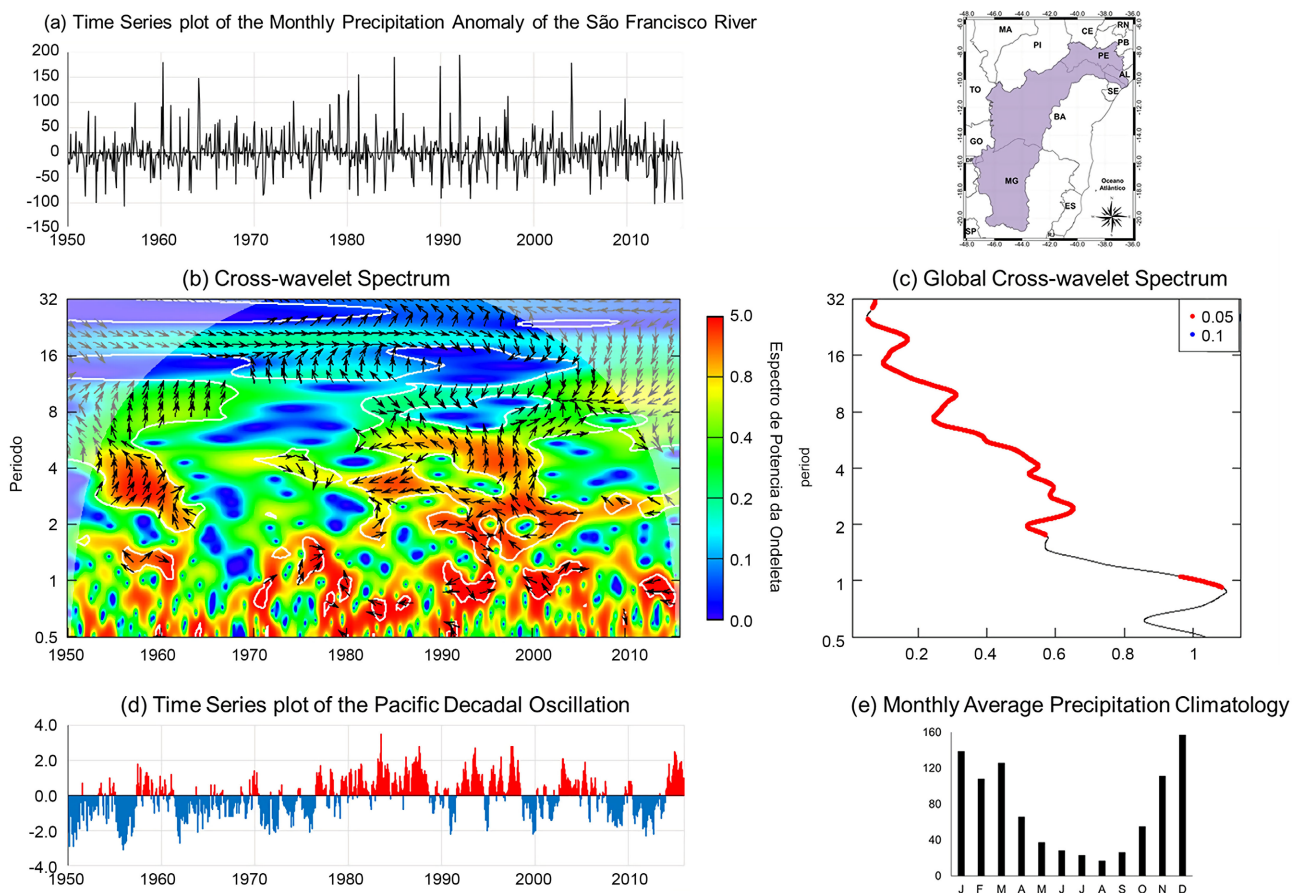


**Figure 16.** Similar to **Figure 15** but for the Pacific Decadal Oscillation (PDO). Source: Author, 2022.

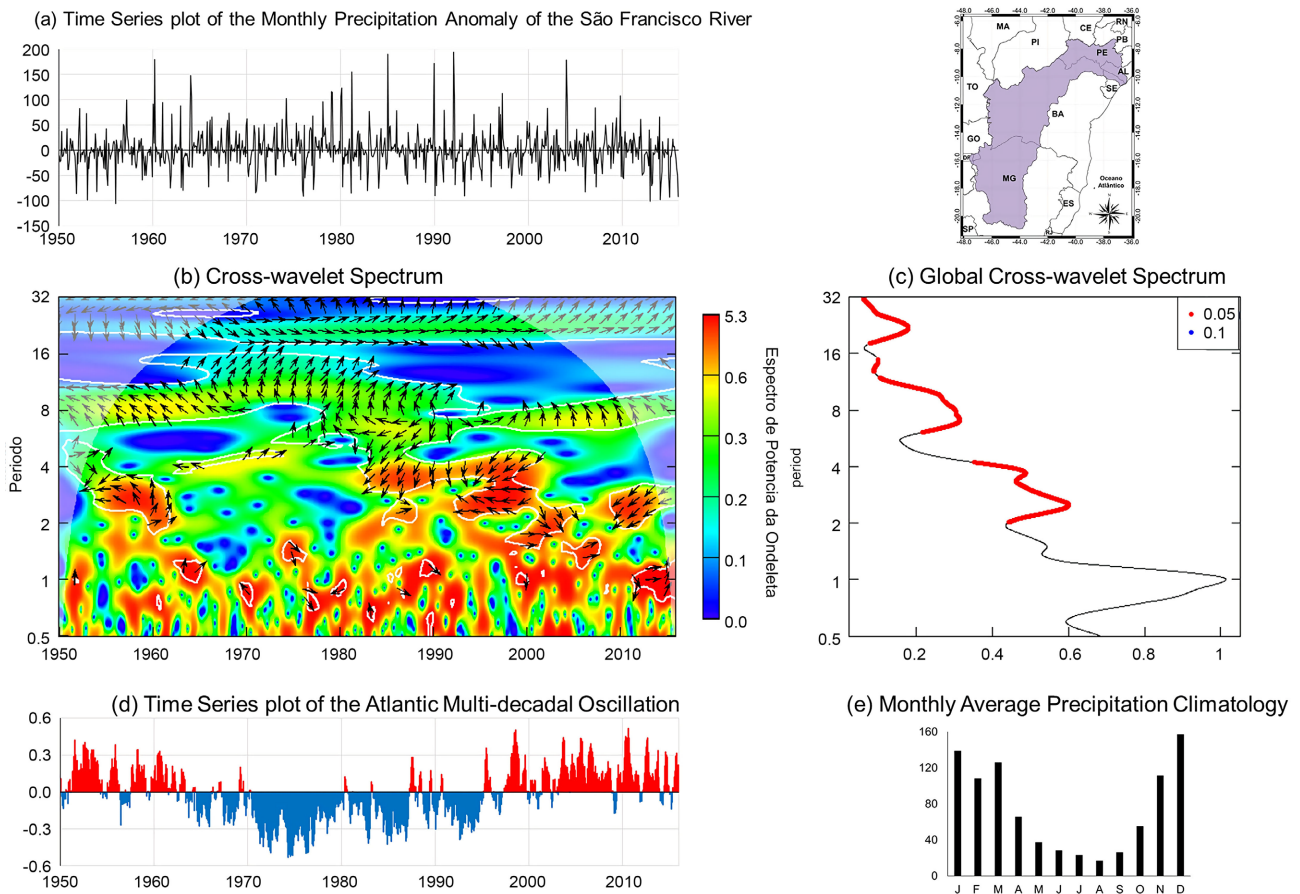


**Figure 17.** Similar to **Figure 15** but for Atlantic Multidecadal Oscillation (AMO). Source: Author, 2022.

During the positive phase of the AMO, the anomalies moved opposite to each other until the middle of the 50s. After that, the anomalies were in phase. Within the 7-year to 11-year cycles, they were continuously out of phase until the end of the 60s. The high-frequency power spectra variability between the 80s and 2000s indicated the anomalies were out of phase with the precipitation leading until 1993 when this signal was reversed, giving rise to an opposite response between them. In the early 2000s, they moved together, but over time the AMO led over the precipitation. Between 2010 and 2015, the annual cycle was in phase, but with alternating signals. The AMO led soon after moving together. Already in mid-2014 and 2015, the precipitation led. And between 2-year and 4-year cycles, the precipitation anomaly led.

**Figure 18** shows few signs with high variability, especially between the intra-seasonal to annual cycles, 2 to 4 years and 22 years. In the 6-month and one-year cycles, the anomaly series were out of phase with the NAO leading. In the 70s, the NAO led ahead by three months the precipitation anomaly. In other high power spectra cores, the time series moved opposite to each other, except in the early 70s when they moved along together. Another core of high variability is found in between the 2-year and 4-years that moved together between the 90s and 2000s. There is a response in the 7-year cycle when they moved together

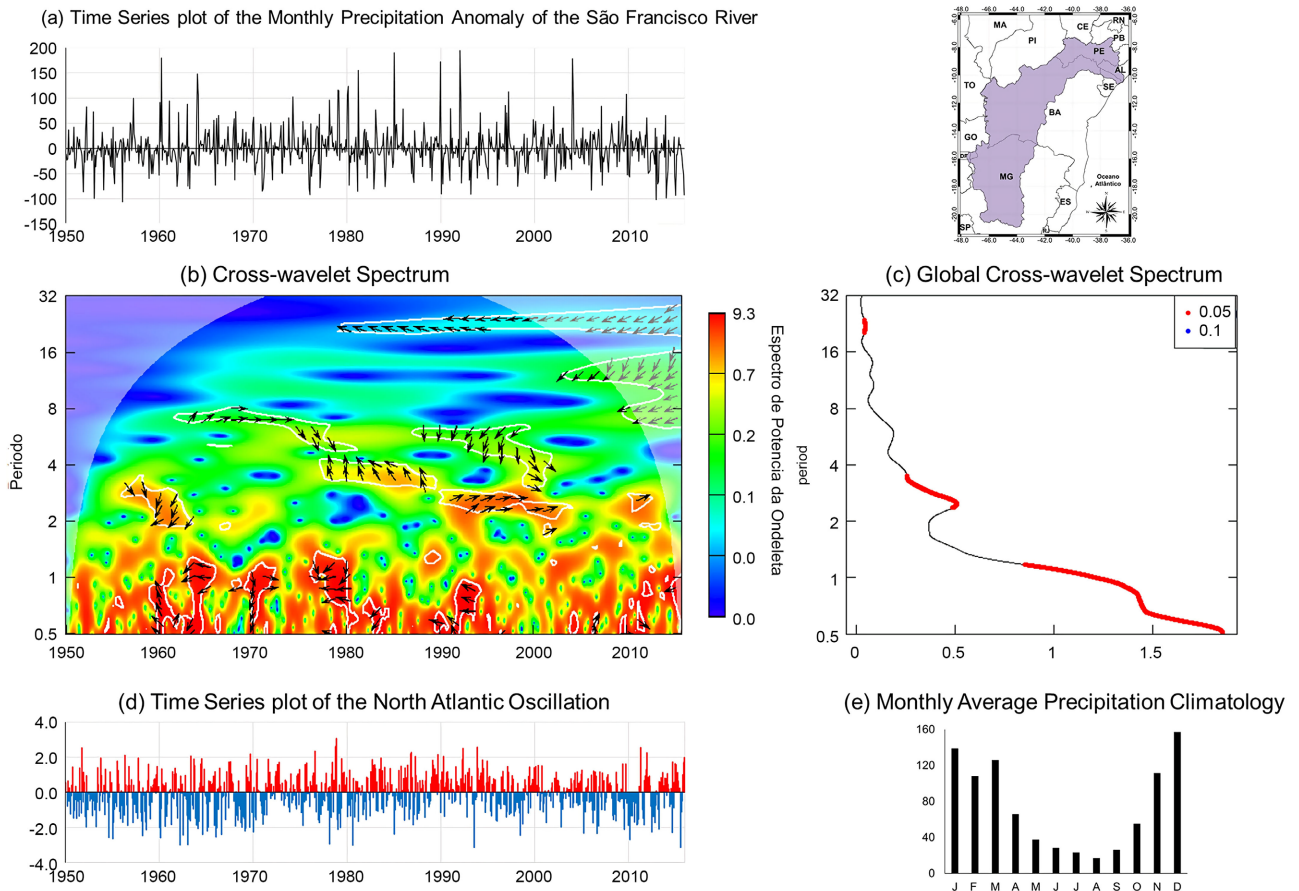


**Figure 18.** Similar to **Figure 15** but for the North Atlantic Oscillation (NAO). Source: Author, 2022.

between the 60s and the first half of the 70s. Shortly after, the NAO led between 1975 and 1980. Between 1980 and 1990, the NAO led in the 22-year cycle that began in 1980, both time series moved opposite to each other.

The remarkable core between the intraseasonal and four-year cycles in the early 50s, in the annual cycle in **Figure 19**, shows the vector pointing to the 4th quadrant that means AD led ( $y$ ) over the precipitation anomaly ( $x$ ) with a negative correlation and in phase up to 3-year periodicity. Between 1955 and 1965, a high-power core is in between the annual and 4-year cycle from the late 50s to 1962. They moved together between 1-year and 2-year cycles with signal changes around 1965 and the DA leading. As it approached the 2-year cycle, the precipitation anomaly was ahead of the AD. In between 2-year and 4-year cycles, the series moved opposite to each other. Another significant core is observed around the 7-year cycle from 1970 to 1983, with a perfectly negative correlation, and the annual cycle tending to move together with the precipitation anomaly leading. The cores between 1990 and 2015 between the intraseasonal and 2-year cycle, shows the precipitation leading, except between 2014 and 2015 with AD leading over the precipitation anomaly. In the 2-year and 4-year cycles, the precipitation anomaly led from the 90s to the 2000s.

**Figure 20** shows another remarkable dominance of the 11-year cycle as well

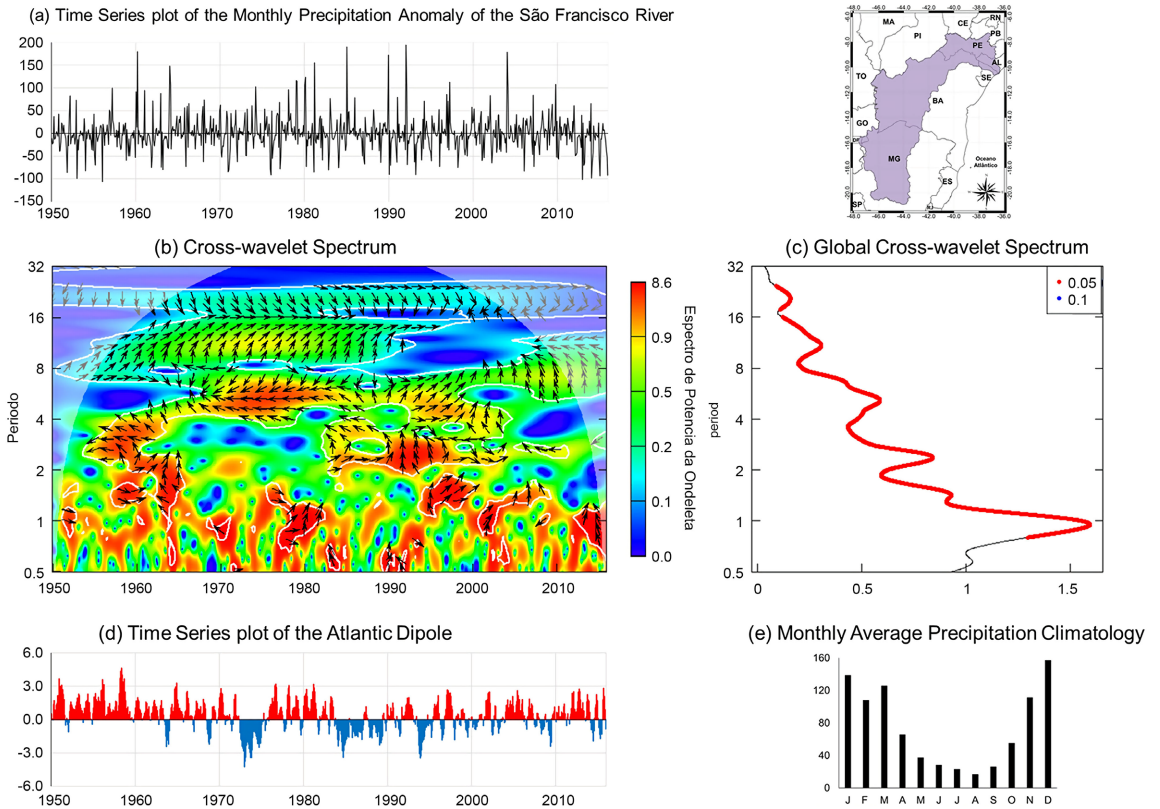


**Figure 19.** Similar to **Figure 15** but for Atlantic Dipole (AD). Source: Author, 2022.

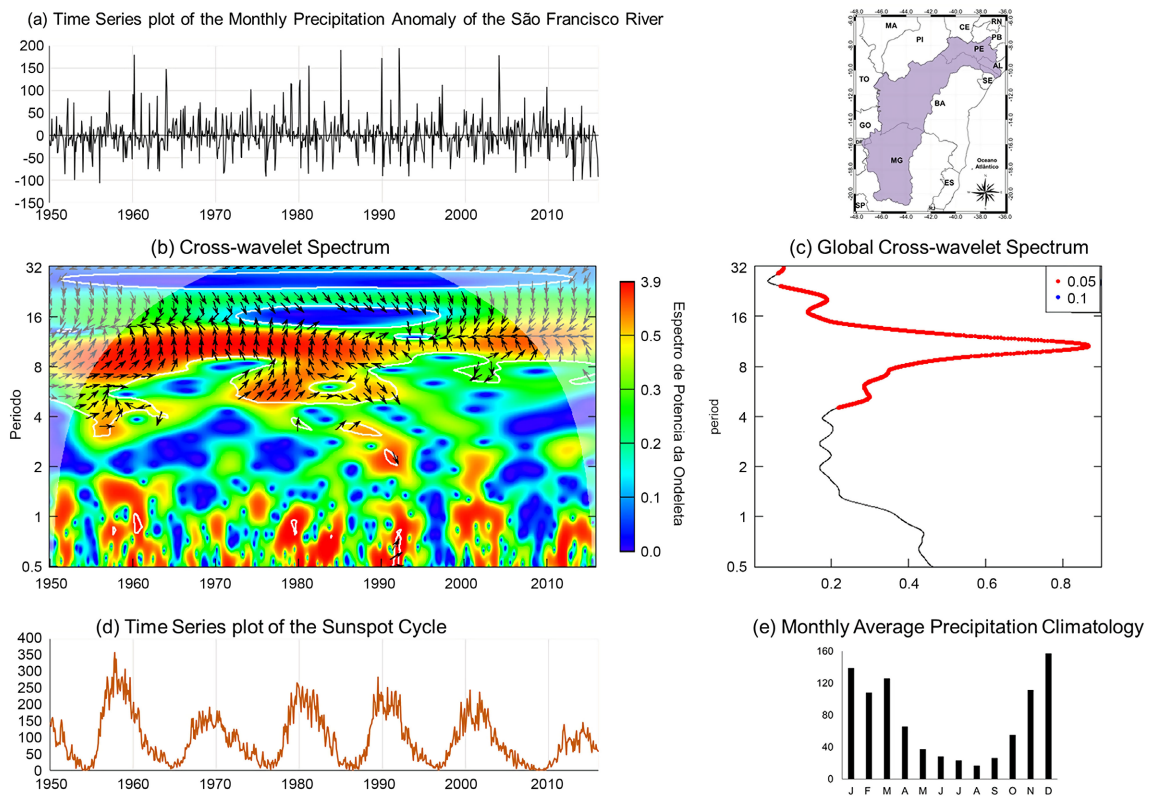


**Figure 20.** Similar to **Figure 15** but for the Number of Sunspots (NS). Source: Author, 2022.

as the annual variability in the 2 to 4-year, 4 to 8-year, and mainly between 8 and 16-year. The precipitation anomaly leads on the time scales between 8 and 16 years until the early 90s. They moved opposite in the late 90s to 2015. On the 4-year and 8-year scales, precipitation anomaly led. On the 4-year time scale, both anomalies moved completely together while around the 7-year cycle they moved opposite to each other.

Therefore, the wavelet analysis indicates high temporal variability in SFRB, especially at time scales between 1-year and 8 years associated with the Atlantic Dipole, North Atlantic Oscillation, and the Oceanic ENSO Index as well as with the number of sunspots between 8-year and 16-years.

## 5. Conclusion

The statical analyses of the SFRB were challenging due to its latitudinal extended and geographic location under the influence of weather systems from the convective scale (e.g., sea breeze) to the large scale (e.g., ITCZ) that result in different precipitation regimes at different spatial-temporal scales. A 65-year long time series of monthly precipitation from 199 selected rain gauges sites was used to establish the SFRB climatology. It indicates a very high spatial-temporal variability. The SPI indicated four main homogeneous regions with consistent patterns in dry and wet seasons. The main component analysis indicated that 87.4% of the total variance of the monthly precipitation average is explained by the first 4 factors as well as defined pattern. The cross-wavelet analysis indicates that the ocean climate indices impact the annual precipitation. There is a significant impact above the 2-year cycle. The cross-wavelet power spectra between the Atlantic Ocean and the Pacific Ocean indices indicated that the Niño Ocean Index and the Atlantic Dipole showed the highest correlation with the SFRB monthly precipitation average anomaly. Further studies are being developed for a season precipitation forecast system based on neural networks.

## Acknowledgements

The authors thank the Agência Nacional de Águas (ANA) for providing the precipitation databases, the Earth System Research Laboratory of the Physical Science Division/National Oceanic and Atmospheric Administration (ESRL/PSD/NOAA) for providing the ocean indices database and the National Geophysical Data Center/National Oceanic and Atmospheric Administration (NGDC/NOAA) for providing number of sunspots database. N.A.S was sponsored by the Coordenação de Aperfeiçoamento de Pessoal de Nível Superior (CAPES) and by Conselho Nacional de Desenvolvimento Científico e Tecnológico (CNPq). A.J. P.F. is a research fellow of CNPq under grant 302349/2017-6.

## Conflicts of Interest

The authors declare no conflicts of interest regarding the publication of this paper.

## References

- [1] Bierkens, M.F.P., Dolman, A.J. and Troch, P.A. (2008) Editors: Climate and the Hydrological Cycle. Special Publication 8, International Association of Hydrological Sciences, United Kingdom.
- [2] Villela, S.M. and Mattos, A. (1975) Applied Hydrology. McGraw-Hill do Brasil, São Paulo, 245 p.
- [3] Wisler, C.O. and Bratter, E.F. (1964) Hydrology. To the Technical Book. Rio de Janeiro, 484 p.
- [4] Collischonn, W. and Tassi, R. (2009) Introducing Hydrology. Institute for Hydraulic Research. Universidade Federal do Rio Grande do Sul, Porto Alegre.
- [5] Schiavetti, A. and Camargo, A.F.M. (2002) Watershed Concepts: Theories and Applications. Editus-Editora da UESC, Ilhéus, 293 p.
- [6] Tucci, C.E.M. (1998) Hydrological Models. ABRH Editora da UFRGS, Porto Alegre, 669 p.
- [7] Portugal, W. and Pacinin, A.A. (2013) The Influence of Galactic Cosmic Rays on Earth's Climate. *Revista Univap (Special Edition)*, **19**, 21-26.  
<https://revista.univap.br/index.php/revistaunivap/article/view/235>
- [8] Marengo, J.A. (2009) Impacts of Weather and Climate-Related Extremes—Social and Economic Impacts. In: *Bulletin of the Climate Change Research Group—GPMC*, Special Edition, INPE, Cachoeira Paulista, SP, Brasil, 1-5.  
[http://mudancasclimaticas.cptec.inpe.br/~rmclima/pdfs/newsletters/Boletim\\_No8\\_Port.pdf](http://mudancasclimaticas.cptec.inpe.br/~rmclima/pdfs/newsletters/Boletim_No8_Port.pdf)
- [9] Galvão, J. and Bermann, C. (2015) Water Crisis, and Energy: Conflicts in the Multiple Uses of Water. *Advanced Studies*, **29**, 43-68.  
<https://doi.org/10.1590/S0103-40142015000200004>
- [10] Silva Dias, M.A.F. (2014) Extreme Weather Events. *USP Magazine*, No. 103, 33-40.  
<https://doi.org/10.11606/issn.2316-9036.v0i103p33-40>
- [11] Santos, N.A., Siqueira, A.H.B., Bezerra, K.L.T., Castro, C.P.Q. and Melo, M.L.D. (2011) Extreme Events: Analysis of the Event Occurred in June 2010 on the East Coast of Northeastern Brazil. *Proceedings of the 17th Brazilian Congress of Agro-meteorology*. XVII CBAGRO, Guarapari, ES, 2011, 5 p. <http://www.sbagro.org/>
- [12] Bellprat, O., Lott, F.C., Gulizia, C., Parker, H.R., Pampuch, L.A., Pinto, I., Ciavarella, A. and Stott, P.A. (2015) Unusual Past dry And Wet Rainy Seasons over Southern Africa and South America from a Climate Perspective. *Weather and Climate Extremes*, **9**, 36-46. <https://doi.org/10.1016/j.wace.2015.07.001>
- [13] Reboita, M.S., Gan, M.A., Da Rocha, R.P. and Ambrizzi, T. (2010) Rainfall Regimes in South America: A Bibliographic Review. *Brazilian Journal of Meteorology*, **25**, 185-204. <https://doi.org/10.1590/S0102-77862010000200004>
- [14] Brasil, M.M.A. (2006) Notebook of the São Francisco Hydrographic Region. Ministry of the Environment, Department of Water Resources, Brasília.
- [15] National Water Agency (2019) São Francisco Hydrographic Region: Waters That Contribute to the Development of 521 Municipalities.  
<http://www2.ana.gov.br/Paginas/portais/bacias/SaoFrancisco.aspx>
- [16] Reboita, M., Krusche, N., Ambrizzi, T. and Rocha, R. (2012) Understanding Weather and Climate in South America. *Terra e Didática*, **8**, 34-50.  
<https://doi.org/10.20396/td.v8i1.8637425>
- [17] Regional Environmental Protection Agency of the Rio Grande Basin (2020) River Grande Basin. <https://arpariogrande.org.br/>



- [18] Pereira Filho, A.J., Vemado, F., Vemado, G., Reis, F., Giordano, L., Cerri, R., Santos, C., Lopes, E., Gramani, M., Ogura, A., Zaine, J., Cerri, L., Augusto Filho, O., Da Fonseca, F. and Amaral, C. (2018) A Step towards Integrating Cmorph Precipitation Estimation with Rain Gauge Measurements. *Advances in Meteorology*, **2018**, Article ID: 2095304. <https://doi.org/10.1155/2018/2095304>
- [19] Minas Gerais Energy Company (2020) River Grande Basin. <https://www.cemig.com.br/wp-content/uploads/2021/05/ras-2020.pdf>
- [20] Bier, A.A. and Ferraz, S.E.T. (2017) Comparison of Gap Filling Methodologies in Meteorological Data for Stations in Southern Brazil. *Brazilian Journal of Meteorology*, **32**, 215-226. <https://doi.org/10.1590/0102-77863220008>
- [21] Paulhus, J.L.H. and Kohler, M.A. (1952) Interpolation of Missing Precipitation Records. *Monthly Weather Review*, **80**, 129-133. [https://doi.org/10.1175/1520-0493\(1952\)080%3C0129:IOMPR%3E2.0.CO;2](https://doi.org/10.1175/1520-0493(1952)080%3C0129:IOMPR%3E2.0.CO;2)
- [22] Horton, R.E. (1917) Rational Study of Rainfall Data Makes Possible Better Estimates of Water Yield. *Engineering News-Record*, **79**, 211-213.
- [23] Ferreira, D.F. (2011) Multivariate Statistics. 676 p. 2nd Edition, Revisada e ampliada, Editora UFLA, Lavras.
- [24] Wilks, D.S. (2006) Statistical Methods in the Atmospheric Sciences. 2nd Edition, International Geophysics Series, Academic Press, Cambridge, MA, 649 p.
- [25] SETOSA—Principal Component Analysis. <http://goo.gl/0VHKtW>
- [26] Lorenz, E. N. (1956) Empirical Orthogonal Functions, and Statistical Weather Prediction. Massachusetts Institute of Technology, Department of Meteorology, Cambridge.
- [27] Albuquerque, M.F., Souza, E.B., Oliveira, M.C.F. and Souza Júnior, J.A. (2010) Precipitation in the Mesoregions of the State of Pará: Climatology, Variability and Trends in Recent Decades (1978-2008). *Brazilian Journal of Climatology*, **6**, 151-168. <https://doi.org/10.5380/abclima.v6i0.25606>
- [28] Silva, T.R. (2019) Precipitation in the Rio Grande-Rs (1913-2016): Descriptive and Variability Analysis. Master's Dissertation, Postgraduate Program Course in Geography (PPGGEO), Institute of Human Sciences and Information (ICHI), Federal University of Rio Grande (FURG), Rio Grande, 90p.
- [29] Vieira, P.C. and Bolzan, M.J.A. (2008) Espectro Cruzado de Ondeleita Aplicada na Variação Solar Medida pelo Satélite SOHO. *Physicae (APGF)*, **7**, 21-23.
- [30] Oda, T.O. (2010) Analysis of Interannual Variability of Cabo Frio Coastal Upwelling through Cross Wavelets. *Proceedings of XVI Brazilian Congress of Meteorology*, Belém, 2011.
- [31] Varanis, M.V.M. and Pederiva, R. (2011) Time Series Correlation Detection Using Wavelet Cross Spectrum and Wavelet Coherence. *X Brazilian Conference on Dynamics, Control and Applications (Dincon)*, Águas de Lindóia, São Paulo, SP, 2011, 711-714. <http://arquivo.sbmec.org.br/dincon/2011/download.php>
- [32] Blain, G.C. and Kayano, M.T. (2011) 118 Years of Monthly Data from the Standardized Precipitation Index: Meteorological Series from Campinas, State of São Paulo. *Brazilian Journal of Meteorology*, **26**, 137-148. <https://doi.org/10.1590/S0102-77862011000100012>
- [33] Veeda, D., Montagne, R. and Araujo, M. (2012) Cross-Wavelet Bias-Corrected by Normalizing Scales. *Journal of Atmospheric and Oceanic Technology*, **29**, 1401-1408. <https://doi.org/10.1175/JTECH-D-11-00140.1>
- [34] Rösch, A. and Schmidbauer, H. (2018) WaveletTOCmp 1.1: A Guided Tour through the R Package. 2-59.

- [35] Rösch, A. and Schmidbauer, H. (2014) WaveleTOComp: A Guided Tour through the R-Package. 1-38.
- [36] Vacha, L. and Barunik, J. (2012) Co-Movement of Energy Commodities Revisited: Evidence from Wavelet Coherence Analysis. *Energy Economics*, **34**, 241-247. <https://doi.org/10.1016/j.eneco.2011.10.007>
- [37] Auth, C. (2013) Continuous Wavelet Transform, and Wavelet Coherence—Implementation and Application to the Diversification Analysis of Hedge Fund Returns. [https://www.nag.com/about/student\\_awards/christoph-auth-nag-student-award.pdf](https://www.nag.com/about/student_awards/christoph-auth-nag-student-award.pdf)
- [38] Haniff, N.M. and Masih, M. (2016) Shariah Stocks as an Inflation Hedge in Malaysia. *Munich Personal RePEc Archive*.
- [39] Naghettini, M. and Pinto, É. J. de A. (2007) Statistical Hydrology. Companhia de Pesquisa de Recursos Minerais, Belo Horizonte, MG.
- [40] De Oliveira, M.R.P. and Galvani, E. (2017) Extreme Precipitation Events in the Longitudinal Profile Paraty (RJ)-Campos do Jordão (SP). *Journal of the Department of Geography*, 58-66. <https://doi.org/10.11606/rdg.v0ispe.133419>
- [41] Mckee, T.B., Doesken, N.J. and Kleist, J. (1993) The Relationship of Drought Frequency and Duration to Time Scales. *Proceedings of the 8th Conference on Applied Climatology*, Anaheim, 17-22 January 1993, 179-184.
- [42] Blain, G. C., Pezzopane, J. R., Pezzopane, J. E. and Bonomo, R. (2010) Standardized Precipitation Index Applied to Drought Conditions in the State of Espírito Santo. *Brazilian Journal of Agricultural and Environmental Engineering*, **14**, 1067-1073. <https://doi.org/10.1590/S1415-43662010001000007>
- [43] Centro de Previsão de Tempo e Estudos Climáticos (CPTEC) of Instituto Nacional de Pesquisas Espaciais (INPE) (2022) Standardized Precipitation Index (SPI). <http://clima1.cptec.inpe.br/spi/pt>
- [44] European Drought Observatory (EDO) (n.d.) Standardized Precipitation Index (SPI). Copernicus European Drought Observatory (EDO). <https://edo.jrc.ec.europa.eu/>
- [45] Calisto Acosta, O.E. (2014) Informação hidrometeorológica na regulação do setor elétrico brasileiro: Indicadores de avaliação de disponibilidade hídrica. Relatório Final de Projeto de Pesquisa de Pós-Doutorado, Universidade de São Paulo, São Paulo, 71 p.